Electron diffraction study of crystal structures of (Sr$_{1-x}$Ba$_x$)$_2$Nb$_2$O$_7$

Bikas Aryal,[1,*] Daisuke Morikawa,[1] Kenji Tsuda,[2] Shinya Tsukada,[3] Yukikuni Akishige,[3] and Masami Terauchi[1]

[1]*Institute of Multidisciplinary Research for Advanced Materials, Tohoku University, 2-1-1 Katahira, Aoba-ku, Sendai 980-8577, Japan*
[2]*Frontier Research Institute for Interdisciplinary Sciences, Tohoku University, Aramaki aza Aoba 6-3, Aoba-ku, Sendai 980-8578, Japan*
[3]*Faculty of Education, Shimane University, Matsue 690-8504, Japan*

Selected-area electron diffraction and convergent-beam electron diffraction (CBED) techniques are used to reveal the Ba doping effect on the crystal structure of (Sr$_{1-x}$Ba$_x$)$_2$Nb$_2$O$_7$ [SBN(x)] in the temperature range from 293 to 693 K. Ba doping of Sr$_2$Nb$_2$O$_7$ (SN) causes weakening of the incommensurate modulation and deviation from the C-centered lattice. On the other hand, symmetries of fundamental reflections in CBED patterns of SBN(x) are seen to be the same as those of SN, showing a small structural deviation from $Cmc2_1$. Crystal symmetries above and below the temperature of a relaxorlike dielectric anomaly in SBN ($x = 0.32$) at 465 K remain unchanged. CBED experiments with a nanometer-sized electron probe do not show any indication of the presence of a nanodomain around this temperature. However, the presence of a few-micron-sized polar-inversion domains is found at around 573 K in SBN ($x = 0.32$). The origin of the reported relaxorlike dielectric anomaly in SBN ($x = 0.32$) is discussed on the basis of the experimental results of CBED.

I. INTRODUCTION

Strontium niobate, Sr$_2$Nb$_2$O$_7$ (SN), is a well-known ferroelectric and piezoelectric material characterized by an exclusively high Curie temperature, $T_c = 1615$ K [1–3]. Thus, it is a potential candidate for high-temperature piezoelectric sensing applications, which are of great importance in chemical and material processing and automotive, aerospace, and power-generating industries [4–6]. The unique properties of SN such as the low coercive field, low permittivity, and high-heat resistance enable it to be used in Pb-free nonvolatile ferroelectric memory devices based on field effect transistors and capacitors and optical waveguides [7–9].

SN belongs to a family of oxide compounds having the chemical formula A$_n$B$_n$O$_{3n+2}$ [10,11]. The crystal structure of SN (A$_n$B$_n$O$_{3n+2}$; $n = 4$) is comprised of slabs with a distorted perovskite-type octahedral framework stacked along the b axis and separated by planes of additional oxygen atoms [10–12]. In the high-temperature paraelectric phase above $T_c = 1615$ K (phase I) [3], the space group was reported to be $Cmcm$, in analogy with the paraelectric phase of Sr$_2$Ta$_2$O$_7$ [13]. In the ferroelectric phase below T_c (phase II) [3], the confirmed space group is $Cmc2_1$ [14] and spontaneous polarization $\mathbf{P}_s$ appears along the orthorhombic c axis [1–3]. SN also undergoes an incommensurate phase transition at $T_i = 488$ K [15]. Below this temperature (phase III), the structure is modulated with the wave vector of $\mathbf{q} = (\frac{1}{2} - \delta)\boldsymbol{a}^*$ [16], where δ and $\boldsymbol{a}^*$ are a temperature-dependent misfit parameter and a reciprocal lattice vector corresponding to the averaged crystal structure. The modulated structure in this phase III was explained by the rotation of the NbO$_6$ octahedron about the b axis [17,18]. The value of δ decreases upon cooling, from 0.022 at 488 K to

0.008 at 55 K, without reaching 0 [16]. At room temperature (RT), the space group $Pbn2_1$ was reported by making an assumption ($a = 2a_0$ if $\delta = 0$) [19]. Furthermore, at $T_L = 117$ K [3], another ferroelectric phase transition takes place. Below T_L (phase IV), a new component of the spontaneous polarization appears along the b axis, resulting in $\mathbf{P}_s$ lying in the bc plane [20]. The space group $Pb11$ was proposed for phase IV from infrared measurements [21]. In this article, Ba-doped SN, (Sr$_{1-x}$Ba$_x$)$_2$Nb$_2$O$_7$, is abbreviated SBN(x), where x indicates the Ba content.

Ba doping of SN was attempted with the aim of enhancing ferroelectric and piezoelectric properties [22] around the morphotropic phase boundary. However, the composition phase diagram of SBN(x) ceramics has not yet been reported. For SBN(x) ceramics, a decrease in T_c according to an increase in the amount of Ba doping was identified in the 1970s [3]. Since then, there has been great effort to investigate the Ba doping effect on phase transitions at T_i and T_L, incommensurate modulation, crystal structure, and ferroelectric and piezoelectric properties of SN [22–26]. Raman scattering measurement for SBN ($x = 0.32$) suggested cell doubling below 543 K and a new structural phase transition around this temperature [25]. On the other hand, a relaxorlike dielectric anomaly in SBN ($x = 0.32$) at around $T_m = 465$ K was reported from a dielectric constant measurement [26]. The relation of the two new phase transition temperatures from these different experiments has not yet been clarified. Also, the origin of this relaxorlike dielectric anomaly is currently unknown. It is noted that a typical relaxor-type dielectric anomaly was reported for (Sr$_{1-x}$Ba$_x$)Nb$_2$O$_6$, which has a tetragonal tungsten bronze structure and is known as a uniaxial relaxor ferroelectric [27]. Akishige *et al.* investigated the Ba doping effect on the crystal structure of SN using x-ray diffraction and disclosed the disappearance of incommensurate reflections in SBN ($x = 0.32$) [26]. However, the Ba doping effect in

*bikasaryal141@gmail.com

incommensurate modulation of SN for other SBN(x) ceramics compositions with $x \leqslant 0.16$ is still unknown.

In this study, the Ba doping effect on the incommensurate modulation, unit cell size, and crystal symmetries of SN has been investigated using selected-area electron diffraction (SAED) and convergent-beam electron diffraction (CBED) techniques. Crystal symmetries of SBN ($x = 0.32$) above and below the relaxorlike dielectric anomaly [26] and the origin of this dielectric anomaly are also discussed.

II. EXPERIMENTAL PROCEDURE

Single crystals of SBN(x) with $x = 0.0$, 0.16, and 0.32 were grown in an O_2 gas flow by a floating zone method using an FZ furnace [26]. Transmission electron microscopy specimens were prepared in the following manner. First, a piece of a single crystal was crushed into tiny segments and dispersed into ethanol. Then the suspension was dropped onto microgrids for electron microscopy. A JEM-2010 transmission electron microscope (TEM) was used to obtain SAED and CBED patterns and dark-field (DF) images. Another TEM, JEM-2010FEF, which is equipped with a field-emission gun and an Omega-type energy filter, was used to check the existence of nanometer-scale domains in SBN ($x = 0.32$). Both instruments were operated at an accelerating voltage of 100 kV. A double-tilt specimen-heating holder was used to control the specimen's temperature. Specimens were examined in the temperature range from RT to 693 K, with a temperature step of 30 K. The nominal spot size of the electron probe used to obtain CBED patterns was approximately 10 nm for JEM-2010 and 1 nm for JEM-2010FEF.

III. RESULTS AND DISCUSSION

Figures 1(a)–1(c) are the SAED patterns of SN, SBN ($x = 0.16$), and SBN ($x = 0.32$), respectively, taken at [010] incidence and RT. The intensity of incommensurate spots of SN, indicated by arrows, becomes weak and broad at $x = 0.16$ and almost disappears at $x = 0.32$. The appearance of very weak diffraction spots, enclosed in circles in Fig. 1(a), has been explained by double reflection of incommensurate reflections in the zeroth-order Laue zone (ZOLZ) [17,18]. These can be indexed as $1 \pm 2\delta$ 0 0. Similarly, Figs. 1(b) and 1(c) show weak intensities at $h0l$ (h:odd) positions, but they cannot be explained by the double reflection because there is no long-range periodicity of incommensurate modulation. These weak intensities are kinematically forbidden for the C-centered lattice. This indicates deviation of the crystal lattices of SBN ($x = 0.16$ and 0.32) from the C-centered lattice. This result suggests that the space group $Cmc2_1$ for SBN ($x = 0.32$) is not appropriate even for the averaged structure. There are two possible reasons for the deviation from the C-centered lattice. One is the distortion of the crystal lattice resulting from the difference in the ionic radii of Ba and Sr atoms. The other is the imperfect kinematical extinction rule according to the different scattering amplitudes of Ba and Sr atoms.

Figures 2(a)–2(c) show CBED patterns taken at [010] incidence and RT from SN, SBN ($x = 0.16$), and SBN ($x = 0.32$), respectively. The strong fundamental reflections of the ZOLZ and the first-order Laue zone (FOLZ) in Fig. 2(a) show mirror
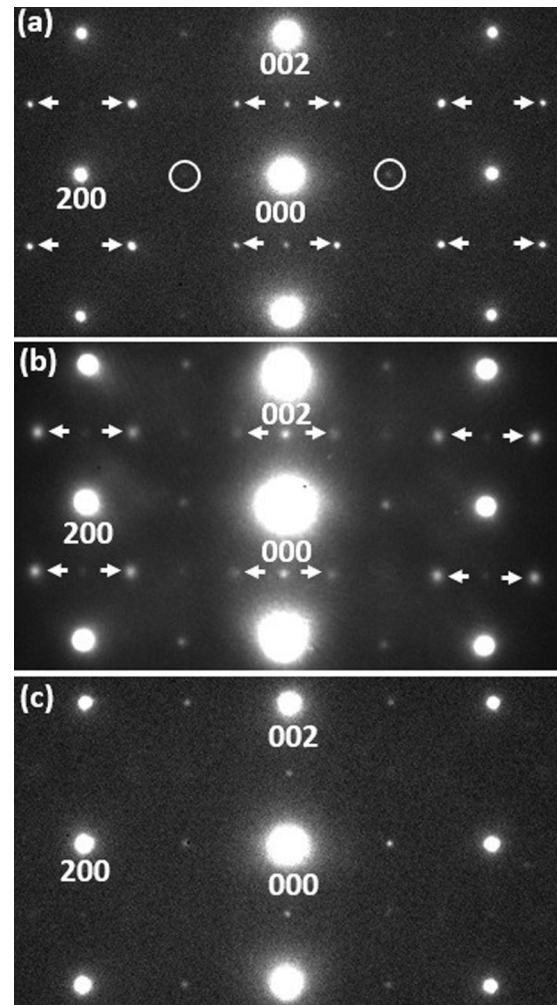

FIG. 1. SAED patterns taken at [010] incidence and RT from (a) SN, (b) SBN ($x = 0.16$), and (c) SBN ($x = 0.32$). Arrows indicate incommensurate reflections. Weak $h0l$ (h:odd) reflections in (b) and (c) represent the deviation of the crystal lattice of SBN ($x = 0.16$ and 0.32) from the C-centered lattice.

symmetry perpendicular to the a axis. On the other hand, the incommensurate reflections, indicated by black arrows in Fig. 2(a), do not show mirror symmetry perpendicular to the a axis. The symmetry of the incommensurate reflections can be understood by $(3 + 1)$-dimensional symmetry [28]. In Fig. 2(b) and Fig. 2(c), the fundamental reflections [neglecting symmetries of very weak $h0l$ (h:odd) reflections] also show mirror symmetry perpendicular to the a axis. Figures 2(d)–2(f) show CBED patterns taken at [110] incidence and RT from SN, SBN ($x = 0.16$), and SBN ($x = 0.32$), respectively. Each pattern was taken under the 005 excitation condition. In Fig. 2(d), the 005 reflection disk shows dark cross lines parallel and perpendicular to the 005 diffraction vector corresponding to the A_2 and B_2 dynamical extinction lines, respectively. This indicates the existence of a 2_1-screw axis along the c axis. In Figs. 2(e) and 2(f), A_2 and B_2 dynamical extinction lines are also seen in the 005 reflection disks. The CBED symmetries shown in Fig. 2 have been confirmed for more than 15 SN, SBN ($x = 0.16$), and SBN ($x = 0.32$) crystal segments. Also, the CBED symmetries as well as the intensity
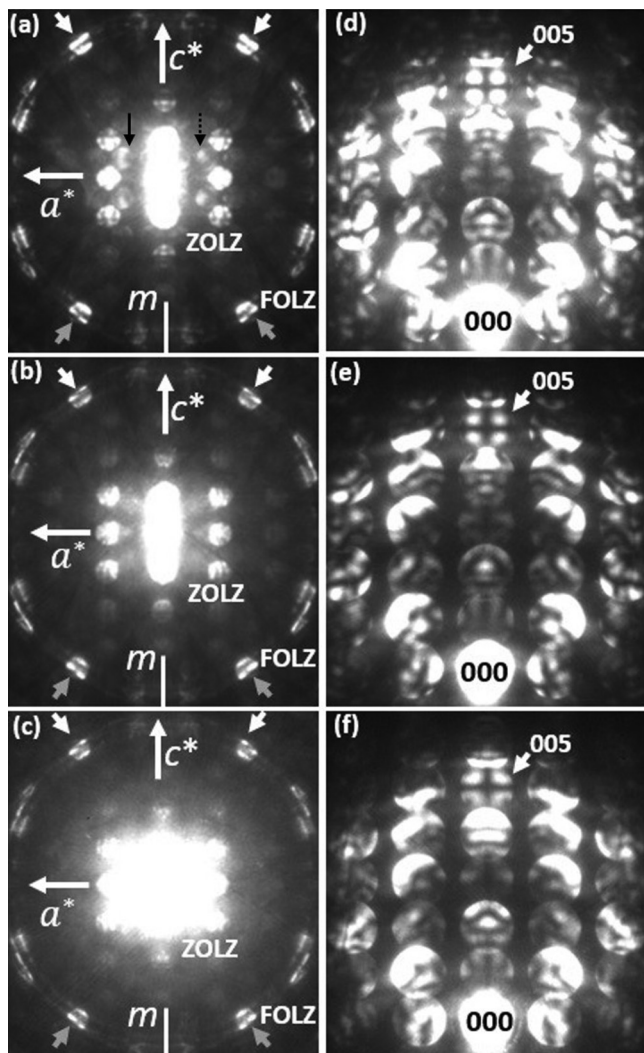
FIG. 2. CBED patterns taken at [010] incidence and RT from (a) SN, (b) SBN ($x = 0.16$), and (c) SBN ($x = 0.32$). CBED patterns of (d) SN, (e) SBN ($x = 0.16$), and (f) SBN ($x = 0.32$) were taken at [110] incidence and RT by exciting 005 reflection. Strong fundamental reflections in (a)–(c) show symmetry m perpendicular to [100], owing to the space group $Cmc2_1$. Incommensurate reflections indicated by black arrows in (a) do not show the symmetry m perpendicular to the [100] direction. The appearance of A_2- and B_2-type dynamical extinction lines (black cross lines on 005 reflection disks) in (d)–(f) indicates that the 2_1-screw axis along the c axis of SN remains almost unchanged by Ba doping.

FIG. 3. Schematic representation of the orientation of the NbO$_6$ octahedral layers in (a) SN, (b) SBN ($x = 0.16$), and (c) SBN ($x = 0.32$) when the crystal structure is viewed along [010]. Black arrows indicate the direction of tilt of the NbO$_6$ octahedron about the b axis. The unit cell of the averaged structure is depicted as the shaded region.

distribution in CBED disks were found to be the same before and after the exposure time. These CBED symmetries in Fig. 2 indicate that the fundamental reflection symmetries m perpendicular to the a axis and 2_1-screw axis along the c axis of the structure are almost unaffected by Ba doping. Hence, Ba doping to SN causes a weakening of incommensurate modulation and a deviation from the C-centered lattice, but the averaged crystal symmetry remains almost unchanged. This indicates very slight structural deviation from the $Cmc2_1$ phase.

It was reported that incommensurate reflections in SN originated from rotations of the NbO$_6$ octahedron about the b axis
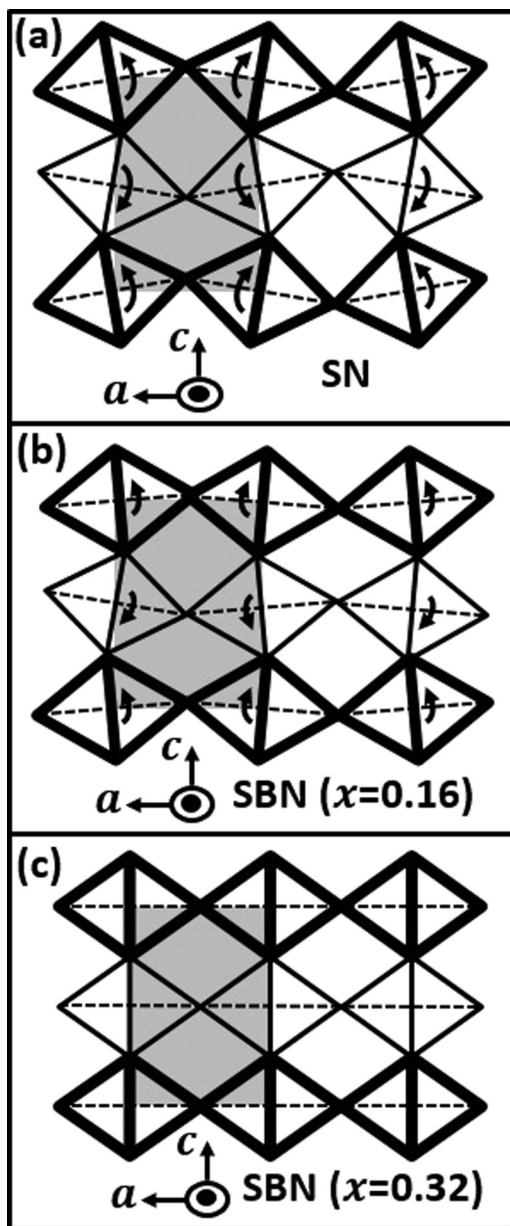
as schematically shown in Fig. 3(a) [17], which represents a schematic arrangement of NbO$_6$ octahedrons viewed along the [010] direction. Black arrows and the shaded region show the directions of tilt of the octahedron and a unit cell of the averaged structure, respectively. Thus, a simple model which can explain the decrease in the incommensurate reflection intensities in SBN ($x = 0.16$) is a decrease in the rotation angle in the NbO$_6$ octahedron as depicted in Fig. 3(b). The near-disappearance of the incommensurate reflection in SBN ($x = 0.32$) may correspond to Fig. 3(c). An x-ray study reported that 32% Ba doping of SN results in an expansion of

the unit cell volume by 3.15% [26]. Thus, the cell volume of SBN ($x = 0.16$) might be between those of SN and SBN ($x = 0.32$). The lattice parameters of SBN ($x = 0.32$) are larger than those of SN by 1.7%, 0.8%, and 0.7% in the *a*, *b*, and *c* directions, respectively. The larger cell volume and lattice constants should be due to the replacement of Sr atoms with larger Ba atoms. The larger lattice constants of *a* and *c* of SBN ($x = 0.32$) can be related to a decrease in the rotation angle of the NbO_6 octahedron about the *b* axis, which can be related to the disappearance of incommensurate reflection spots as shown in Fig. 1(c). This simple model is also consistent with the unchanged crystal symmetry *m* perpendicular to the *a* axis in SBN ($x = 0.16$ and 0.32). On the other hand, a simple decrease in the tilt angle of the NbO_6 octahedron as in Fig. 3 cannot explain either the larger expansion in the *a* direction than the *c* direction or the expansion in the *b* direction. Then the resultant structural change upon Ba doping may be composed not only by a smaller rotation of the NbO_6 octahedron as in SN but also by a distortion of the NbO_6 octahedron due to a statistical occupation of the larger Ba atom. Thus, to explain the anisotropic lattice parameter change, distortion of the NbO_6 octahedron must be considered. Details of the effect of Ba doping on tilt and distortion of the octahedron are expected to be clarified by quantitative crystal structure analysis using CBED.

From dielectric constant measurement, it was reported that SBN ($x = 0.32$) shows a relaxorlike dielectric anomaly at around $T_m = 465$ K [26]. The origin of this relaxorlike behavior is still unknown. In usual relaxor materials, it has been known that there exist nanoscale domains [29] having random orientations. Thus, a CBED experiment with an electron probe 1 nm in diameter was conducted for SBN ($x = 0.32$) in the temperature range from RT to 545 K, with a temperature step of 30 K, to examine the presence of nanometer-scale domains. It is to be noted that these are the nominal temperatures of the specimen holder. The symmetries of CBED patterns of SBN ($x = 0.32$) were found to be the same even using a probe size 10 nm and/or 1 nm in diameter. In the CBED patterns obtained in this temperature range, a change or lowering of symmetries was not found, suggesting the absence of nanometer-sized domains. Thus, a CBED experiment was conducted at a temperature higher than 545 K. Figures 4(a)–4(c) represent CBED patterns obtained at [010] incidence and 573 K from different positions of a crystal segment of SBN ($x = 0.32$). Figure 4(d) shows the DF image corresponding to the $00\bar{2}$ reflection obtained at 573 K. The positions where the CBED patterns in Figs. 4(a)–4(c) were obtained are indicated by black dots numbered 1, 2, and 3 in the DF image in Fig. 4(d). The CBED patterns in Figs. 4(a) and 4(c) show 180° polarity reversal by referring to the intensity distribution of the 200 and $\bar{2}00$ reflection disks, as indicated by arrows. The intensity distribution indicated by arrows in Fig. 4(b) shows an overlapping of Figs. 4(a) and 4(c), suggesting that position 2 in Fig. 4(d) is the overlapping region of two inversion domains assigned in Figs. 4(a) and 4(c). Figure 5(a) shows the CBED patterns taken at [010] incidence from SBN ($x = 0.32$) at $T = 693$ K $> T_m$. This pattern shows symmetry *m* perpendicular to the *a* axis, which is the same symmetry as that at RT $< T_m$ as shown in Fig. 2(c). Furthermore, the 2_1-screw axis along the *c* axis also remained unchanged as indicated in Fig. 5(b),
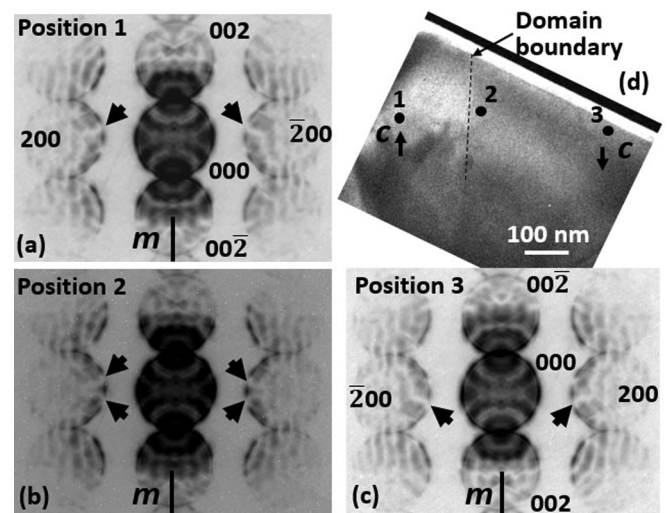

FIG. 4. CBED patterns taken at [010] incidence from SBN ($x = 0.32$) at 573 K from (a) the first domain, (b) overlapping domains near the domain boundary, and (c) the second domain. (d) DF image corresponding to the $\bar{2}00$ reflection showing the area where these CBED patterns were obtained. Black arrows at the 200 and $\bar{2}00$ reflection disks in (a) and (c) indicate the characteristic intensity distribution, from which the polarity reversal can be identified easily. The dotted black line in the DF image indicates the ferroelectric domain boundary.

which shows the A_2 and B_2 dynamical extinction lines in the 005 reflection disk as observed for RT $< T_m$, which is shown in Fig. 2(f). Hence, despite the relaxorlike broad dielectric anomaly at $T_m = 465$ K, the crystal symmetries above and below this temperature remained unchanged. These results indicate that the broad dielectric anomaly in SBN ($x = 0.32$) at around 465 K is not due to a relaxor-type phase transition.

In relaxor ferroelectric materials such as $Pb(Zn_{1/3}Nb_{2/3})O_3$ and $Pb(Mg_{1/3}Nb_{2/3})O_3$ [29–31], the broad dielectric anomaly appears to be due to the randomness in electric and strain fields resulting from the chemical disorder and difference in the ionic charge and radius of B-site atoms. In SBN(x), Sr atoms at the A site have been replaced with Ba atoms. As Sr and Ba atoms have the same ionic charge, +2, there is no randomness of ionic charge at the A site. On the other hand, the existence of two types of
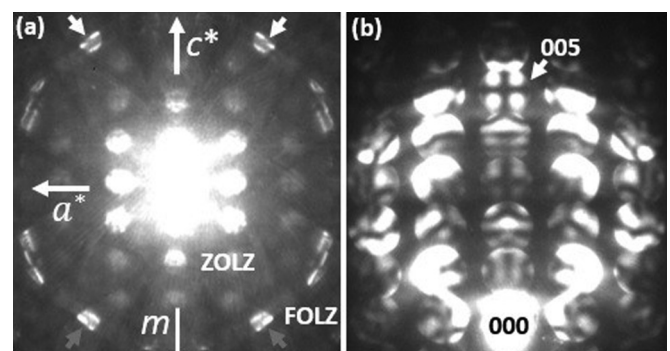

FIG. 5. CBED patterns taken from SBN ($x = 0.32$) at $T = 693$ K $> T_m$ at (a) [010] incidence and (b) [110] incidence.

random fields has been expected in SBN ($x = 0.32$) [26]. The first is a random strain field due to the difference in the ionic radius of Ba^{2+} and Sr^{2+} ions. However, randomness of the strain field might be small because symmetries of CBED patterns were almost unaffected. The second type is a random electric field due to O vacancies created by the migration of O vacancies because of Ba doping. To check the increase in O vacancies due to Ba doping, a quantitative elemental analysis using EDS was done. However, there is no clear evidence for an increase in O vacancies (a decrease in oxygen content) due to Ba doping. To clarify the increase in O vacancies, it is better to use a spectroscopy method sensitive to electronic structure [32–34] in combination with theoretical calculations of electronic states.

A Raman scattering experiment which probes local bonding structures reported that unit cell doubling of SBN ($x = 0.32$) occurs below 543 K [25]. If there is long-range order of cell doubling, additional spots should exist at 1/2 0 0 or 0 0 1/2 in the SAED pattern in Fig. 1(c) and/or additional higher-order Laue zone reflections between the ZOLZ and the FOLZ in the CBED pattern in Fig. 2(c). However, no additional diffraction intensities were observed. This experimental result shows no long-range order of cell doubling of SBN ($x = 0.32$) along the a, b, and c axes below 543 K, though it does not eliminate the possibility of local cell doubling.

IV. CONCLUSION

In this study, SAED and CBED techniques were used to investigate the Ba doping effect on the crystal structure of SBN(x) and identify the origin of the relaxorlike dielectric anomaly in SBN ($x = 0.32$). Ba doping causes a weakening of incommensurate modulation with the maintenance of the averaged crystal symmetry of $Cmc2_1$. Taking account of lattice expansion in the a, b, and c directions, Ba doping should cause not only a decrease in the tilt angle of the NbO_6 octahedron corresponding to the near-disappearance of incommensurate reflections in SBN ($x = 0.32$) but also a distortion of the NbO_6 octahedron network. A small deviation from the C-centered lattice caused by Ba doping has been found for the first time. CBED studies show that there is no indication of a nanometer domain and no change in crystal symmetry above and below the reported relaxorlike dielectric anomaly temperature. Thus, the broad dielectric anomaly in SBN ($x = 0.32$) is not due to a relaxor-type phase transition. To clarify the Ba doping effect on the crystal structure other than the disappearance of incommensurate modulation, quantitative crystal structure refinement is strongly expected. The relaxorlike behavior may be due to randomness in SBN(x). For identification, it is necessary to use spectroscopic techniques such as electron energy-loss spectroscopy [32,33] and soft x-ray emission spectroscopy [34], which are sensitive to electronic structure.

ACKNOWLEDGMENTS

[1] S. Nanamatsu, M. Kimura, K. Doi, and M. Takahashi, J. Phys. Soc. Jpn. **30**, 300 (1971).

[2] M. Takahashi, S. Nanamatsu, and M. Kimura, J. Cryst. Growth **13**, 681 (1972).

[3] S. Nanamatsu, M. Kimura, and T. Kawamura, J. Phys. Soc. Jpn. **38**, 817 (1975).

[4] H. Ning, H. Yan, and M. J. Reece, J. Am. Ceram. Soc. **93**, 1409 (2010).

[5] H. Yan, H. Zhang, M. J. Reece, and X. Dong, Appl. Phys. Lett. **87**, 082911 (2005).

[6] H. Yan, H. Zhang, R. Ubic, M. J. Reece, J. Liu, Z. Shen, and Z. Zhang, Adv. Mater. **17**, 1261 (2005).

[7] A. Ishitani and M. Kimura, Appl. Phys. Lett. **29**, 289 (1976).

[8] Y. Fujimori, N. Izumi, T. Nakamura, and A. Kamisawa, Jpn. J. Appl. Phys. **37**, 5207 (1998).

[9] Y. Fujimori, T. Nakamura, and A. Kamisawa, Jpn. J. Appl. Phys. **38**, 2285 (1999).

[10] F. Lichtenberg, A. Herrnberger, K. Wiedenmann, and J. Mannhart, Prog. Solid State Chem. **29**, 1 (2001).

[11] F. Lichtenberg, A. Herrnberger, and K. Wiedenmann, Prog. Solid State Chem. **36**, 253 (2008).

[12] P. Daniels, R. Tamazyan, C. A. Kuntscher, M. Dressel, F. Lichtenberg, and S. V. Smaalen, Acta Cryst. B **58**, 970 (2002).

[13] N. Ishizawa, F. Marumo, T. Kawamura, and M. Kimura, Acta Cryst. B **32**, 2564 (1976).

[14] N. Ishizawa, F. Marumo, T. Kawamura, and M. Kimura, Acta Cryst. B **31**, 1912 (1975).

[15] K. Ohi, M. Kimura, H. Ishida, and H. Kakinuma, J. Phys. Soc. Jpn. **46**, 1387 (1979).

[16] N. Yamamoto, K. Yagi, G. Honjo, M. Kimura, and T. Kawamura, J. Phys. Soc. Jpn. **48**, 185 (1980).

[17] N. Yamamoto, Acta Cryst. A **38**, 780 (1982).

[18] N. Yamamoto and K. Ishizuka, Acta Cryst. B **39**, 210 (1983).

[19] K. Scheunemann and K. H. Muller-Buschbaum, J. Inorg. Nucl. Chem. **37**, 1679 (1975).

[20] K. Ohi and S. Kojima, Jpn. J. Appl. Phys. **24**, 817 (1985).

[21] E. Buixaderas, S. Kamba, and J. Petzelt, J. Phys.: Condens. Matter **13**, 2823 (2001).

[22] Z. Gao, H. Ning, C. Chen, R. Wilson, B. Shi, H. Ye, H. Yan, and M. J. Reece, J. Am. Ceram. Soc. **96**, 1163 (2013).

[23] A. Hushur, Y. Akishige, and S. Kojima, Ceram. Int. **30**, 2023 (2004).

[24] G. Shabbir, Y. Akishige, and S. Kojima, Sci. Technol. Adv. Mater. **6**, 656 (2005).

[25] A. Hushur, Y. Akishige, and S. Kojima, Mater. Sci. Eng. B **120**, 45 (2005).

[26] Y. Akishige, S. Tsukada, and I. Takahashi, J. Phys. Soc. Jpn. **83**, 073601 (2014).

[27] P. Ondrejkovic, M. Kempa, J. Kulda, B. Frick, M. Appel, J. Combet, J. Dec, T. Lukasiewicz, and J. Hlinka, Phys. Rev. Lett. **113**, 167601 (2014).

[28] M. Terauchi and M. Tanaka, Acta Cryst. A **49**, 722 (1993).

[29] A. A. Bokov and Z. G. Ye, J. Mater. Sci. **41**, 31 (2006).

[30] G. Burns and B. A. Scott, Solid State Commun. **13**, 423 (1973).

[31] G. Burns and F. H. Dacol, Solid State Commun. **48**, 853 (1983).

[32] A. Sumiyoshi, H. Hyodo, Y. Sato, M. Terauchi, and K. Kimura, Solid State Sci. **47**, 68 (2015).

[33] D. A. Muller, N. Nakagawa, A. Ohtomo, J. L. Grazul, and H. Y. Hwang, Nature **430**, 657 (2004).

[34] H. Urushiyama, H. Morito, H. Yamane, and M. Terauchi, RSD Adv. **8**, 40505 (2018).